# Phase imaging without $2\pi$ ambiguity by multiwavelength digital holography

**J. Gass, A. Dakoff, and M. K. Kim**

*Department of Physics, University of South Florida, Tampa, Florida 33620*

Received January 13, 2003

We present a phase-imaging method with an axial range that can in principle be arbitrarily large compared to the wavelength and does not involve the usual phase unwrapping by detection of phase discontinuity. The method consists of the generation and combination of two phase maps in a digital holography system by use of two separate wavelengths. For example, we reconstructed the surface of a spherical mirror with ~10-nm axial resolution and an axial range of ~3 $\mu$m. © 2003 Optical Society of America

*OCIS codes:* 180.3170, 120.5050, 180.6900, 090.1760, 090.2880.

In digital holography, the holographic interference pattern is digitally sampled by a CCD camera and the image is numerically reconstructed by application of the results from diffraction theory.[1] Digital holography offers a number of significant advantages such as the availability of both amplitude and phase information on the optical field and versatility of the processing techniques that can be applied to the complex field data.[2] For example, interferometric deformation measurement consists simply of subtraction of two numerically reconstructed fields.[3] In microscopy applications[4–6] the reconstructed image can be numerically focused to any plane in the object. Phase imaging is particularly straightforward in digital holography and leads to images with an axial resolution of a fraction of wavelength.[7] However, the phase images contain $2\pi$ discontinuities for objects of optical depths greater than the wavelength. Most of the phase-unwrapping algorithms for removal of the discontinuities require subjective intervention when there are height steps on the object that are more than a wavelength.[8]

In this Letter we present a phase-imaging method with an axial range that can in principle be arbitrarily large compared to the wavelength and does not involve the usual phase unwrapping by detection of phase discontinuity. This method includes the generation and combination of two phase maps in a digital holography system by use of two separate wavelengths. For example, we have reconstructed the surface of a spherical mirror with ~10-nm axial resolution and an axial range of ~3 $\mu$m.

The basic principle of multiwavelength phase imaging is described in Fig. 1, which illustrates the numerical values that were used in generating the simulation plots. Suppose that the object is a slanted plane of height $h = 5.0$ $\mu$m, as shown in Fig. 1(a). The vertical axis is 5.0 $\mu$m full scale in Figs. 1(a)–1(c) and 1(e)–1(h); in Fig. 1(d) the vertical range is $-2\pi$ to $+2\pi$. A single-wavelength phase image has $2\pi$ discontinuity wherever the height is a multiple of the wavelength. For a wavelength $\lambda_1 = 0.532$ $\mu$m or $\lambda_2 = 0.633$ $\mu$m, phase map $\phi_m(x)$ $(m = 1, 2)$ converted to surface profile $z_m(x) = \lambda_m \varphi_m / 2\pi$ will consist of a number of ramps of height equal to the wavelength, as shown in Figs. 1(b) and 1(c). Subtraction of the two phase maps $\phi_{12}' = \varphi_1 - \varphi_2$ has numerous discontinuities of $2\pi$ [Fig. 1(d)], but adding $2\pi$ wherever $\varphi_{12}' < 0$ yields a new phase map $\phi_{12}(x)$, with a longer range free of discontinuities. In fact the new phase map is equivalent to that of a longer beat wavelength $\Lambda_{12} = \lambda_1 \lambda_2 / |\lambda_1 - \lambda_2| = 3.33$ $\mu$m, and the corresponding surface profile is $z_{12}(x) = \Lambda_{12} \varphi_{12}(x) / 2\pi$, shown in Fig. 1(e). By proper choice of the two wavelengths, axial range $\Lambda_{12}$ can be adjusted to any value that would fit the axial size of the object being imaged.

This technique will provide a straightforward and efficient phase-imaging method in a wide range of applications. A limitation is that any phase noise in each single-wavelength phase map is amplified by a factor equal to the magnification of the wavelengths. Suppose that the single-wavelength phase maps $\phi_m(x)$ contain phase noise $2\pi\epsilon_m$, or that surface profiles $z_m(x)$ have a noise level $\epsilon_m \lambda_m$. The noise in the difference phase map, $\phi_{12}(x)$, is $2\pi\epsilon_{12} = 2\pi(\epsilon_1 + \epsilon_2)$,

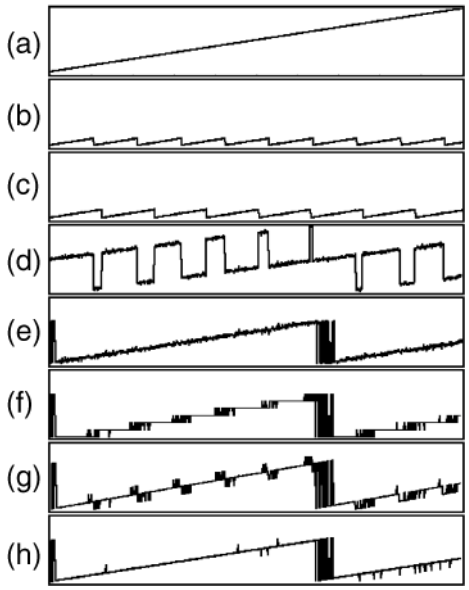


Fig. 1. Simulation of two-wavelength phase imaging. See text for details.

0146-9592/03/131141-03$15.00/0 

and that in the surface profile, $z_{12}(x)$, is $\epsilon_{12}\Lambda_{12}$. The noise has in effect been amplified by approximately a factor of $2\Lambda_{12}/\lambda_m$, as can be seen from a comparison of Fig. 1(e) with Fig. 1(b) or 1(c), where we use $\epsilon_1 = \epsilon_2 = 5\%$. The other half of the phase-imaging method consists of an algorithm to reduce the noise to the level of the single-wavelength phase maps. First, in Fig. 1(f) the surface height $z_{12}(x)$ is divided into integer multiples of one of the wavelengths, say, $\lambda_1$. Then we paste the wavelength-high segments of the single-wavelength surface map $z_1(x)$ from Fig. 1(b) into the steps of Fig. 1(f) to obtain Fig. 1(g). This almost recovers surface profile $z_{12}(x)$ with significantly reduced noise, except at the boundaries of wavelength intervals, where the noise in the single-wavelength phase map causes numerous jumps of size $\pm\lambda_1$. If the noise level is not excessive, most of the spikes in the last step can be removed simply by comparison of Fig. 1(g) with the coarse map of Fig. 1(e) and, if the difference is more than half of $\lambda_1$, addition or subtraction of one $\lambda_1$, depending on the sign of the difference. Figure 1(h) shows the final result as a fine map; the remaining spikes are due to places where the noise in the coarse map is more than one half of $\lambda_1$. That is, the maximum noise level for the method to work properly is given approximately by $\epsilon_m < \lambda_m/4\Lambda_{12} \sim 4\%$, which means that the value of 5% used in the simulation is near the boundary where the noise begins to be excessive.

We now describe experimental achievement of multiwavelength phase imaging. The experimental apparatus depicted in Fig. 2 is an interferometer that has been set up for digital holography. The input laser beam is from either a He–Ne laser (633 nm) or a doubled Nd:YAG laser (532 nm), which are combined by a beam combiner (not shown). The input laser beam is split at beam splitter BS1 into reference and object beams, and each part is focused by lens L1 ($f = 15$ cm) or L2 ($f = 20$ cm) onto focal point F1 or F2. Point F2 is also the front focus of objective L3, so the object is illuminated with a collimated beam. The light scattered from the object travels through BS2 and BS3 and reaches the CCD camera. The reference beam's focus F1 is equidistant from BS3 as F2, so it is optically equivalent to a collimated beam incident from the left of objective L3. Lenses L3 ($f = 10$ cm) and L4 ($f = 15$ cm) provide microscopic magnification: Plane S is imaged by L3 onto S′, which is at the front focus of L4, so the camera focused at infinity records a magnified image of the interference pattern of the light scattered from the object onto S, through a distance $z_o$, and a plane-wave reference wave that would be present at S. In addition, having a separate path for the reference beam as shown facilitates alignment for off-axis holograms. An example of recording and reconstruction by digital holography is shown in Fig. 3.

Figure 3(a) is an in-focus image of a 1.06 mm × 1.06 mm area of a U.S. Air Force resolution target, aluminum coated onto glass with lines of 177-$\mu$m width. Figure 3(b) shows holographic interference between the diffracted object beam ($z_o = 18$ mm) and the off-axis (2.5° horizontally) reference beam. The holographic image of the object is then numerically calculated from the interference pattern by a Huygens diffraction formula.[9] The off-axis arrangement avoids the twin-image problem and helps to reduce intensity and phase noise in the reproduced images. One of the most significant advantages of digital holography is the fact that once the complex electric field of the object is calculated, its amplitude and phase maps [Figs. 3(c) and 3(d)] are readily available in numerical form for further manipulation and processing.

The experimental achievement of multiwavelength phase imaging is demonstrated in Fig. 4. Figure 4(a) is a cross section of a phase map, such as Fig. 3(d), obtained with $\lambda_1 = 532$ nm. The vertical axis is 3.5 $\mu$m full scale for the entire Fig. 4. The number of $2\pi$ discontinuities shows that the reflective object is tilted by ~3.7 $\mu$m in optical path length. We can draw this conclusion only because we have *a priori* knowledge of the general shape of the object, which is a flat glass plate with an aluminum-film coating. The phase discontinuity and ambiguity are removed by the combination of the phase map with another of a second

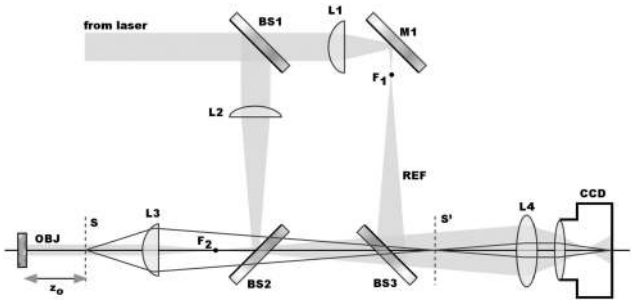


Fig. 2. Apparatus for off-axis digital holographic microscopy experiments. See text for details.

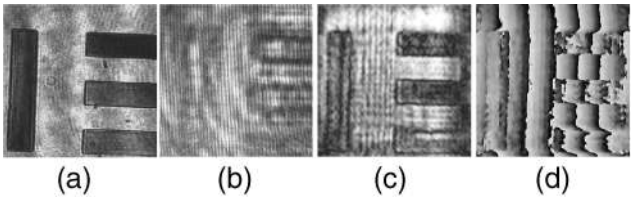


Fig. 3. Digital holography intensity and phase images: (a) object, (b) interference of reference and object waves, (c) intensity image of digital holographic reconstruction, (d) phase image.

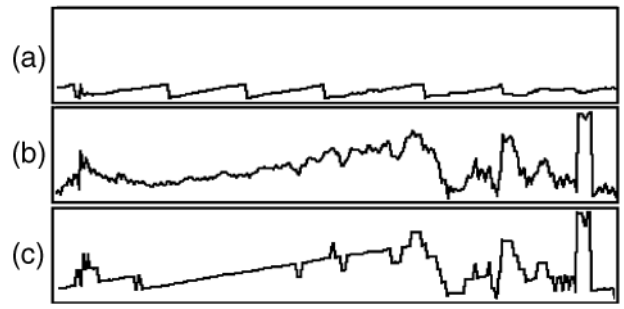


Fig. 4. Experiment of two-wavelength phase imaging: (a) single-wavelength phase profile, (b) coarse-map phase profile of the beat wavelength, (c) fine-map phase profile after the noise-reduction procedure has been applied.

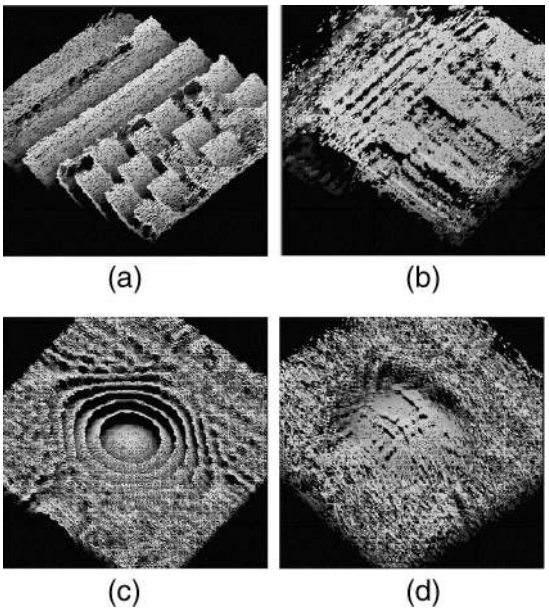


Fig. 5. Reconstructed three-dimensional phase images: (a) single-wavelength and (b) two-wavelength phase images of a reflective resolution target; (c), (d) images of a spherical mirror.

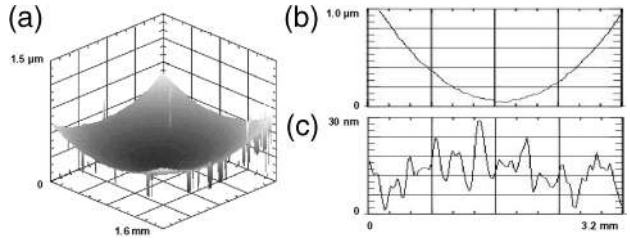


Fig. 6. Noise level in the reconstructed image of a spherical mirror: (a) two-wavelength phase image of a spherical mirror; (b) cross-sectional profile of (a); (c) difference between (b) and a perfect sphere, showing a noise level of the order of 10 nm.

wavelength, $\lambda_2 = 633$ nm (not shown). Following the procedure outlined above, we combined the two phase maps to generate the coarse map of the surface profile shown in Fig. 4(b). Recall that the two wavelengths combine to yield the beat wavelength, 3.3 $\mu$m, and that the coarse map includes amplified phase noise, both of which are evident in Fig. 4(b). The application of a noise-reducing procedure results in the fine map shown in Fig. 4(c), with significant improvement in the reproduction of the flat areas. Some areas of Fig. 4(a) evidently show more than a few percent phase noise, and these areas do not reproduce well in Fig. 4(b) or 4(c), consistent with our estimate above.

The phase maps are presented as three-dimensional plots in Fig. 5. In Fig. 5(a) the single-wavelength phase map has a number of $2\pi$ discontinuities, which are mostly removed in the two-wavelength phase map of Fig. 5(b). The second map still has a significant amount of noise, but it is clear that the method is successful in removing phase discontinuities. We note that the apparent thickness of the aluminum coating was measured, from another view of these data, to be ~75 nm, consistent with a previous result from digital holography.[7] In another set of experiments we imaged the phase fronts of spherical mirrors. For example, Figs. 5(c) and 5(d) are generated from a 1.6 mm $\times$ 1.6 mm area of a spherical mirror. Here Newton's rings of the single-wavelength phase map are merged into a single dome-shaped surface, approximately 750 $\mu$m in diameter and 3 $\mu$m high, in the two-wavelength image. These measurements are consistent with the nominal radius of curvature $R = 40$ mm of the mirror and take into account that the optical path-length variation is twice the physical height of the surface for reflective geometry of the experiment. In another experiment, shown in Fig. 6, we used a spherical mirror with $R = 1200$ mm. Figure 6(a) shows a 1.6 mm $\times$ 1.6 mm area of the image, and Fig. 6(b) shows a particularly noise-free 3.2-mm-long cross section of the mirror. For Fig. 6(c) we fitted a circular arc of radius 1200 mm and plotted the difference, showing that the rms noise level in the surface map is of the order of 10 nm.

These results demonstrate the validity of the principles of phase imaging without $2\pi$ ambiguity by two-wavelength digital holography. Most of the remaining noise probably arises from the surface quality of the various optical components, characterized as $\lambda/20 \sim \lambda/10$, or 5–10% in phase noise. We are extending the method to an iterative procedure of three- or more-wavelength phase imaging, which can further reduce the noise to desired levels. The phase-imaging method presented here should be useful for generating quantitatively accurate three-dimensional images of reflective and transparent objects, such as in the characterization of optical fibers and in real-time imaging of the formation of cell–substrate interfaces during animal cell locomotion.

This research is supported by National Science Foundation grant DBI-9986257. M. K. Kim's e-mail address is mkkim@cas.usf.edu.

## References

1. U. Schnars and W. Jueptner, Measurement Sci. Technol. **13,** R85 (2002).
2. M. K. Kim, Opt. Express **7,** 305 (2000), http://www.opticsexpress.org.
3. S. Seebacher, W. Osten, and W. Jueptner, Proc. SPIE **3479,** 104 (1998).
4. W. S. Haddad, D. Cullen, J. C. Solem, J. W. Longworth, A. McPherson, K. Boyer, and C. K. Rhodes, Appl. Opt. **31,** 4973 (1992).
5. T. Zhang and I. Yamaguchi, Proc. SPIE **3479,** 152 (1998).
6. T. C. Poon, K. B. Doh, B. W. Schilling, M. H. Wu, K. Shinoda, and Y. Suzuki, Opt. Eng. **34,** 1338 (1995).
7. E. Cuche, F. Bevilacqua, and C. Depeursinge, Opt. Lett. **24,** 291 (1999).
8. M. Servin, J. L. Marroquin, D. Malacara, and F. J. Cuevas, Appl. Opt. **37,** 1917 (1998).
9. A. Dakoff, J. Gass, and M. K. Kim, "Microscopic three-dimensional imaging by digital interference holography," J. Electron. Imag. (to be published).